

A NOVEL DICEPN-CLUN-BASED PITTING/CRUSTING RATIO ESTIMATION AND MULTICLASS SKIN CANCER CLASSIFICATION USING DERMOSCOPY IMAGES

N. Jasmine and S. Preetha

Department of Computer Science, Sri Ramkrishna College of Arts and Science for Women, India

Abstract

The patient's lifetime is significantly increased by an early detection of Skin Cancer (SC). Nevertheless, none of the existing works concentrated on analyzing the pitting/crusting ratio. Therefore, this paper proposes an effective Dermoscopy, Deep Incremental Convolutional Elastic-tanh Pooling Neural- Cosinu-sigmoidal Linear Unit Network (DICEPN-CLUN)-based pitting/crusting ratio estimation and multiclass SC classification employing dermoscopy images. Primarily, the International Skin Imaging Collaboration-2019 (ISIC-2019) dataset is gathered and then pre-processed. Afterward, the hair removal process is done, followed by lesion segmentation. Likewise, from the segmented lesions, the 3D heat map is constructed. Similarly, from the dataset, the Metadata is extracted, followed by data pre-processing. Then, the features are extracted. In the meantime, the pitting/crusting region identification and pitting/crusting ratio estimation are carried out. An effective Fuzzy Rational Quadratic Weibull Inference System (FRQWIS) is established to identify the PCR. Lastly, the eight categories of SC are efficiently classified by the proposed DICEPN-CLUN. Hence, the proposed work obtained better outcomes with 99.9046% accuracy.

Keywords:

Skin Cancer (SC), Pitting/Crusting Ratio (PCR), Melanoma, Dermoscopy, Deep Incremental Convolutional Elastic-tanh Pooling Neural- Cosinu-sigmoidal Linear Unit Network (DICEPN-CLUN), Exponential Rotated Happycat Function-UNet (ERHF-UNet), and Lesion Segmentation (LS)

1. INTRODUCTION

Globally, one of the most dangerous cancers that cause widespread health illness is SC [1, 2]. Essentially, genetic and environmental factors cause SC [3, 4]. The most aggressive form of SC is melanoma [5]. To identify the SC, many researchers have established Machine Learning (ML) along with Deep Learning (DL) methodologies [6]. Currently, dermoscopy plays a prime role in classifying SC [7, 8]. To perform SC detection, the prevailing works utilized Convolutional Neural Network (CNN) [9, 10]. Nevertheless, none of the existing studies focused on analyzing the PCR during SC classification. In the prevailing [11], the presence of hair on the skin's surface obscured the important visual features of the lesions. The existing [12, 13] failed to consider important metadata and also struggled to accurately segment the skin lesions owing to the surface curvature. Thus, a novel DICEPN-CLUN-based PCR estimation and multiclass SC classification is proposed in this paper.

The paper is structured as: The related works are exhibited in Section 2, the proposed scheme is derived in Section 3, the proposed model's performance is validated in Section 4, and finally, Section 5 concludes the article.

2. LITERATURE SURVEY

In [12] examined a hybrid ML and DL-based SC classification. Here, the features were inputted to the Support Vector Machine (SVM), which classified the SC efficiently. Nevertheless, owing to the lack of contextual factors, this model was ineffective. Likewise, [14] scrutinized a DL-based multi-classification of SC using Dermoscopic Images (DI). Here, to classify the SC, the CNN was established. This approach had better accuracy. Nevertheless, this model was only suitable for fair-skinned subjects. Additionally, [13] offered an automatic SC classification based on a multi-feature fusion scheme. To perform SC classification, the lesion descriptors were subjected to ML models like SVM. This model had high consistency. Nevertheless, due to the surface curvature, this method was less significant. Moreover, [11] advanced DI-based melanoma detection using DL. To perform melanoma lesion classification, the DCNN was used. This model had higher superiority. However, owing to the presence of hair artifacts, this model was less significant. Similarly, [15] applied a multi-classification of SC based on DL. Primarily, the DI was subjected to the Visual Geometry Group (VGG)-16 and CNN, which classified the SC efficiently. Nevertheless, this model had biased outcomes. Then, [16] utilized Vision Transformer (ViT) and CNN for skin disease classification. Here, the segmentation and augmentation were integrated with ViT. Then, CNN was utilized for skin disease classification. However, diverse skin tones were not considered, thus reducing the overall performance. Meanwhile, in [17], the attention mechanism and Swin Transform were utilized for skin cancer diagnosis. The Hybrid Shifted Window Multi-head Self-Attention (HSW-MSA) technique was utilized to improve the training efficiency. On the other hand, the bias errors were not rectified. Next, the prevailing [18] utilized attention-based Dual-path Feature Fusion (DFF) for automatic skin lesion segmentation. At first, the lesion boundaries were identified. Next, the context learning was done using Multiscale Feature Selection (MFS). The semantic and facial features were integrated using DFF. Yet, the end-to-end detection of lesions was difficult to detect. Moreover, the [19] presented DL-based skin lesion segmentation using skin color bias. The Fitzpatrick technique was utilized for detecting skin tone. Then, by using the U-Net and Deep Neural Network (DNN), the segmentation was carried out. But, the unknown data could not be analyzed. In the meantime, the [20] presented Federated Learning for skin lesion diagnosis. Initially, the skin images were collected, and the features were extracted. Then, the CNN was utilized along with Federated Learning for SC identification. Thus, the model aggregated the global server and updated the SC types for accurate classification. However, the unknown data could not be analyzed properly.

3. PROPOSED FRAMEWORK FOR MULTI-CLASS SKIN CANCER CLASSIFICATION

Here, by using DI, a novel DICEPN-CLUN-based pitting/crusting ratio estimation and multiclass SC classification is implemented. A novel Contrast-Discus Transform Limited Adaptive Histogram Equalization (CDTLAHE) is used to perform contrast enhancement, thereby enhancing the surface features. In Fig.1, the proposed methodology's architecture is given.

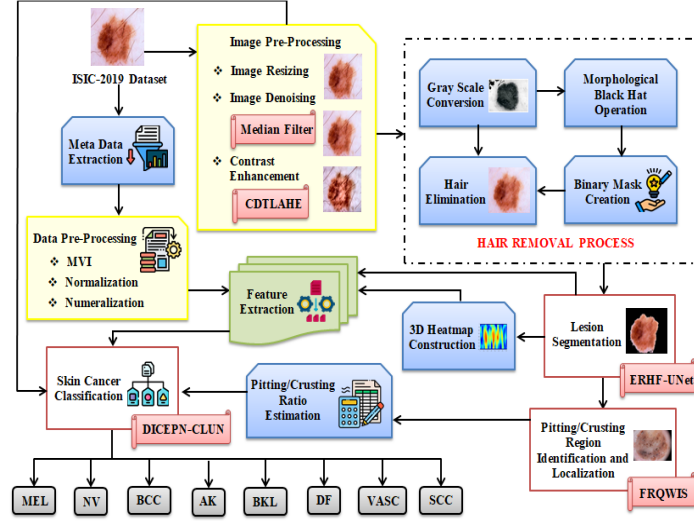


Fig.1. The conceptual framework of the proposed approach

3.1 ISIC-2019 DATASET

Primarily, the ISIC-2019 dataset is gathered. The ISIC-2019 dataset contains a collection of DI ($\partial\delta_h$) regarding various types of SC.

$$\partial\delta_h = \langle \partial\delta_1, \partial\delta_2, \dots, \partial\delta_H \rangle \text{ Here, } h = 1 \text{ to } H \quad (1)$$

Here, H implies the number of input DI.

3.2 IMAGE PRE-PROCESSING

Then, to enhance the model's performance, the $\partial\delta_h$ is pre-processed. The actual dimensions of all the images in the $\partial\delta_h$ is transformed into the same dimensions in image resizing. Next, by using the median filter, the noise presented in the resized images ($\Re\infty$) is eliminated.

$$F^\circ(p, q) = \text{median}\{\mathcal{G}(x, y) | (x, y) \in \Omega_{pq}\} \quad (2)$$

where, F° signifies the filtered value with intensity pixel (p, q) , median specifies the median operation, \mathcal{G} represents the intensity values of the pixel at the location (x, y) in the neighborhood, and Ω_{pq} signifies the window pixel. Then, the $t = 1$ to T number of F° is subjected to the proposed CDTLAHE. The Contrast-Limited Adaptive Histogram Equalization (CLAHE) is computationally efficient. Nevertheless, it has suboptimal enhancement results. Then, to choose the clip limit (ϕ_{lim}), the proposed work introduces the Discus Transform (DT). Primarily,

the filtered image F° is divided into numerous tiles. Next, the histogram (Ψ) is computed.

$$\Psi = F^\circ \cdot \lambda_p, p \forall p \in [0, q-1] \quad (3)$$

$$\phi_{\text{lim}}(F^\circ) = 10^6 (F^\circ)_1^2 + \sum_{t=1}^T (F^\circ)_t^2 \quad (4)$$

$$\Psi^* = \Psi + \frac{\sum_p \Psi(p) - \phi_{\text{lim}+}}{q}; \quad (5)$$

$$\phi_{\text{lim}+} = \max(0, \phi_{\text{lim}})$$

Then, from the clipped histogram (Ψ^*), the normalized cumulative distribution (χ) is calculated.

$$\chi(p) = \frac{1}{D_1 \times D_2} \sum_{t=1}^T \Psi^*(p) \quad (6)$$

where, λ_p denotes the number of pixels, and $D_1 \times D_2$ specify the dimensions. According to $\chi(p)$, each pixel intensity in the tile is mapped to the enhanced intensity level. To form a single enhanced image (Θ), all the interpolated values are combined together.

3.3 HAIR REMOVAL PROCESS

Initially, the Θ is converted into a grayscale image (GV). Next, to highlight the hair, the morphological black hat operation is applied.

$$\beta_{\text{hat}}(GV) = \partial\mathcal{U}(GV, \Phi) - \Xi(GV, \Phi) \quad (7)$$

$$B_{\text{mask}} = \beta_{\text{hat}} \rightarrow \begin{cases} \text{If } (px = 0-40), & \text{hair} \\ \text{If } (px = 41-120), & \text{normal lesions} \end{cases} \quad (8)$$

where, $\partial\mathcal{U}$ and Ξ specify the dilation and erosion operations, respectively, Φ implies the structured element, and β_{hat} signifies the morphed images. Then, by assuming the threshold values, the binary mask (B_{mask}) is created from β_{hat} . To differentiate the hair and normal lesions, the pixel values (px) like (0-40) and (41-120) are assumed, respectively. The hair region is eliminated from Θ based on B_{mask} . Therefore, the hair-removed images are depicted as (γ_\diamond).

3.4 LESION SEGMENTATION

The lesion region is accurately segmented from γ_\diamond based on the proposed ERHF-UNet. The UNet effectively segments the irregular regions. Nevertheless, the UNet has over-segmentation outcomes. Thus, to select the weight (X_{weight}), the proposed method employs the Exponential Rotated Happycat Function (ERHF). Initially, the γ_\diamond is fed into the encoder, which captures contextual features (λ_{map}) via convolution (Conv°).

$$X_{\text{weight}} = Bf_{21} \exp\left(\zeta_{\text{mat}} \frac{5(\gamma_\diamond - of_v)}{100}\right) + M_v \quad (9)$$

$$Conv^{\oplus} = X_{weight} * \lambda_{map} \quad (10)$$

where, Bf_{21} specifies the base function, ζ_{mat} notates the rotation matrix, of_v illustrates the offset vector, and M_v signifies the constant value. Then, the dimensionality-reduced features Rd are transmitted to the bottleneck layer(Bot), which refines the features using the skip connections. Finally, the segmented lesion is mentioned as (\aleph_{∞}) . From the \aleph_{∞} , the 3D heat map (H_{3D}) is created to visualize the intensity values in the three dimensions, which aids in extracting the depth features. The 3D heat map preserves the spatial and contextual depth information. As this map shows volumetric representation, the distinguishing of benign and SC types becomes accurate.

3.5 METADATA EXTRACTION

Similarly, from the ISIC-2019 dataset, the Metadata (K) is extracted, followed by pre-processing. To impute the missing values, the mean values of the non-missing information are used. Then, the feature values are converted into numerical format. Lastly, the numerical features are normalized. For normalization, the Z-score standardization technique, which converts all the features on the same scale, is used. Here, features (\aleph_{Ω}) like compactness, entropy, intensity mapping, color gradient, age, sex, and lesion location are extracted from \aleph_{∞} , H_{3D} , and pre-processed data ζ_{data} .

3.6 PITTING/CRUSTING REGION IDENTIFICATION AND LOCALIZATION

Essentially, the pitting and crusting reflect the depth of depressions and hardened structures, respectively. Here, by using the proposed FRQWIS, the PCR is identified from \aleph_{∞} . The Fuzzy Inference System (FIS) offers precise prediction owing to its adaptability. Nevertheless, the FIS has tuning difficulties. Therefore, to perform fuzzification, the proposed work introduces the Rational Quadratic Weibull Membership (RQWM). In fuzzification, the crisp data is converted into fuzzy data (Fuz).

$$\Gamma_{mem}(\aleph_{\infty}) = \exp\left(-\left(\frac{\aleph_{\infty}}{\tau}\right)^{\alpha}\right) \cdot \frac{1}{1 + (\aleph_{\infty} - \tau)^2 / \alpha^2} \xrightarrow{\text{fuzzification}} Fuz \quad (11)$$

where, Γ_{mem} specifies the RQWM, and τ and α signify the constant values. Next, the fuzzy rules ($\mathcal{R}ule$) are framed as,

$$\mathcal{R}ule = \begin{cases} \text{If } (\varpi = 60-120), & \wp^{\circ} \\ \text{If } (\varpi = 160-255), & \Lambda_i \end{cases} \quad (12)$$

By assuming the pixel value range (ϖ) as 60-120 and 160-255, the pitting (\wp°) and crusting (Λ_i) regions are identified, respectively. The thresholds (60–120 for pitting and 160–255 for crusting) are selected based on histogram analysis of annotated dermatological images, where these intensity ranges consistently represent the respective lesion types. Lastly, in the defuzzification unit, the fuzzy data is converted into crisp data. The pseudocode of proposed FRQWIS is presented below,

Input: Segmented lesions \aleph_{∞}

Output: PCR

Begin

Initialize \aleph_{∞} , Fuz , $\mathcal{R}ule$ and ϖ

For 1 to each \aleph_{∞} do,

Perform fuzzification via RQWM,

$$\Gamma_{mem}(\aleph_{\infty}) = \exp\left(-\left(\frac{\aleph_{\infty}}{\tau}\right)^{\alpha}\right) \cdot \frac{1}{1 + (\aleph_{\infty} - \tau)^2 / \alpha^2} \xrightarrow{\text{fuzzification}} Fuz$$

Execute rule base

$$\mathcal{R}ule = \begin{cases} \text{If } (\varpi = 60-120), & \wp^{\circ} \\ \text{If } (\varpi = 160-255), & \Lambda_i \end{cases}$$

End For

Return (\wp°) and (Λ_i)

End

Next, to localize the regions, the active contour is used. Here, by reducing the energy, the curve moves towards the object boundary (PCR). To capture the surface-level indicators of the lesions, the PCR($\wp c\mathcal{R}$) is estimated from PCR localized data O_{loc} .

$$\wp c\mathcal{R} = O_{loc} \left(\frac{\alpha r(\wp^{\circ})}{Yr(\Lambda_i)} \right) \quad (13)$$

Here, αr and Yr signify the pitting area and area affected by crusting, respectively.

3.7 SKIN CANCER CLASSIFICATION

Lastly, the Θ , \aleph_{Ω} , and $\wp c\mathcal{R}$ are inputted to the proposed DICEPN-CLUN, which classifies the eight types of SC. The DCNN has high scalability. Nevertheless, the DCNN has high computational costs and vanishing gradient issues. Therefore, the proposed method employs the Elastic-tanh Pooling Layer (EPL) (Σ_{pool}) and Cosinu-sigmoidal Linear Unit (CosLU) (μ_{CosLU}). Also, to handle atypical lesions, Incremental Learning (IL) is used. In Fig.2, the proposed DICEPN-CLUN architecture is presented.

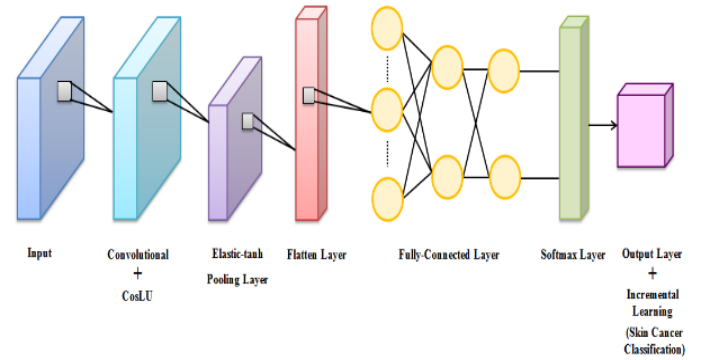


Fig.2. DICEPN-CLUN's architecture

Initially, the inputs $(I\varphi)$, such as Θ , \mathfrak{T}_Ω , and $\wp c\mathfrak{R}$ are fed into the convolutional layer (Cl) , which generates the feature map (η)

$$I\varphi = \{\Theta, \mathfrak{T}_\Omega, \wp c\mathfrak{R}\} \quad (14)$$

$$\mu_{\text{CosLU}}(I\varphi) = (I\varphi + \kappa \cos(\nu I\varphi)) \delta ig(I\varphi) \quad (15)$$

$$Cl = \mu_{\text{CosLU}} * wt \rightarrow \eta \quad (16)$$

$$\Sigma_{\text{pool}}(Cl) = \text{pooling}(\tanh(Cl)) \quad (17)$$

where, κ and ν imply the trainable parameters, and δig represents the sigmoid activation. The CosLU μ_{CosLU} is a non-linear activation function that helps in highlighting the minority class features. It also preserves the class-specific activation. Furthermore, the EPL output Σ_{pool} adapts dynamically to the local feature distribution. The Elastic-tanh pooling improves the stability and avoids sharp changes during backpropagation. Also, it incorporates a hyperbolic tangent non-linearity and boosts the discriminations across the visual patterns. Next, to transform Σ_{pool} into a 1d array (Y) , the flatten operation is applied. Then, the Y is inputted to the fully-connected layer (ω_{ful}) .

$$\omega_{\text{ful}} = \mu_{\text{CosLU}} \cdot (Y \times wt) + \lambda s \quad (18)$$

Lastly, the output layer (Ot) displays the classified SC outcome.

$$\text{Sof}_{\text{max}}(\omega_{\text{ful}}) = \frac{\exp^{\omega_{\text{ful}}}}{\sum_L \exp(\omega_{\text{ful}})_L} \quad (19)$$

$$Ot = [Mel, Nv, Bcc, Ak, Bkl, Df, Vasc, Scc] \quad (20)$$

where, Sof_{max} indicates the softmax function, Mel , Nv , Bcc , Ac , Bkl , Df , $Vasc$ and Scc signify the (1) melanoma, (2) melanocytic nevus, (3) basal cell carcinoma, (4) actinic keratosis, (5) benign keratosis, (6) dermatofibroma, (7) vascular lesion, and (8) squamous cell carcinoma, respectively, wt and λs depict the weight and bias, respectively, and L depicts the number of classes.

Here, Incremental Learning is utilized as a stability-aware update mechanism with metadata-aware feature fusion. The underrepresented skin tones are also processed by Incremental Learning. Hence, the SC classification becomes precise. Also, the EPL that preserves the deep features and CosLU activation, which supports the retention of previously learned representations, encourages smoother parameter updates during new task learning. Hence, this alleviates catastrophic forgetting by reducing the destructive overwriting of parameters during incremental updates. Therefore, the DICEPN-CLUN's pseudo-code is given below,

Input: Θ , \mathfrak{T}_Ω and $\wp c\mathfrak{R}$

Output: Classified SC Ot

Begin

Initialize Θ , \mathfrak{T}_Ω , $\wp c\mathfrak{R}$, μ_{CosLU} and Sof_{max}

For 1 to each input do,

Evaluate convolutional layer, $Cl = \mu_{\text{CosLU}} * wt \rightarrow \eta$

Apply ETP layer $\Sigma_{\text{pool}}(Cl) = \text{pooling}(\tanh(Cl))$

Perform fully-connected layer $\omega_{\text{ful}} = \mu_{\text{CosLU}} \cdot (Y \times wt) + \lambda s$

Execute output layer

End For

Return $Ot = [Mel, Nv, Bcc, Ak, Bkl, Df, Vasc, Scc]$

End

In real-time clinical settings, skin cancer images are collected during the dermatological assessment by using dermoscopic imaging devices, such as digital dermatoscopes (FotoFinder, DermLite, and so on). The dermatologists capture the images of suspicious skin lesions as part of the routine diagnostic workflow. To ensure quality and consistency, the standardized imaging protocols are followed.

- Consistent lighting and magnification for uniform dermoscopic visualization.
- Proper lesion framing and focus to avoid artifacts.
- Metadata annotation, including patient age, sex, lesion location, and preliminary diagnosis.

Before the collection of images, all participating institutions undergo approval by the Institutional Review Board or other equivalent ethics committee's clearance. The clearance is only given to the patient who has given consent for imaging and data usage. Therefore, the proposed work had better efficiency. However, the real-time practical applicability and deployment challenges include:

- Deploying the model across diverse medical centers introduces heterogeneity in hardware capabilities.
- The system is prone to intermittent device connectivity, especially in remote settings. Hence, these device dropouts delay the inconsistency in SC detection.
- Clinical trust is also a challenge due to image sharing.

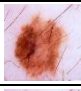




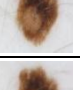
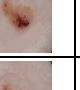

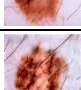



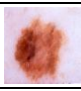
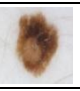





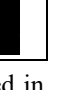




4. RESULTS AND DISCUSSION

4.1 DATASET DESCRIPTION

The proposed approach is tested on the ISIC-2019, HAM10000, and PH² datasets using Python with 80% of the data for training and 20% for testing. The hardware requirements of the proposed system include,

- Processor: Intel i5/core i7
- CPU speed: 3.20 GHz
- OS: Windows 10
- System Type: 64 bit
- RAM: 16 GB
- GPU: NVIDIA GeForce GTX 1660 or AMD Radeon RX 590

Table.1. Image results

Sample / Process	Melanoma	Melanocytic Nevus	Benign keratosis	Vascular lesion
Input				
Resizing				
Denosing				
Contrast enhancement				
HR				
Lesion segmentation				

The image results of the proposed approach are exhibited in Table.1.

4.2 PERFORMANCE ASSESSMENT

Here, the performance analysis is done.

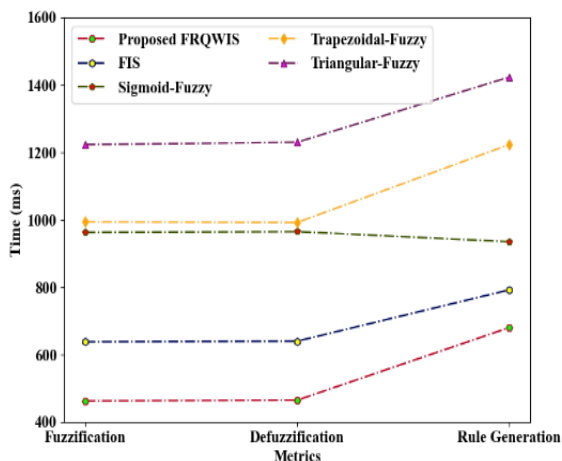


Fig.3. Performance analysis for pitting/crusting region identification

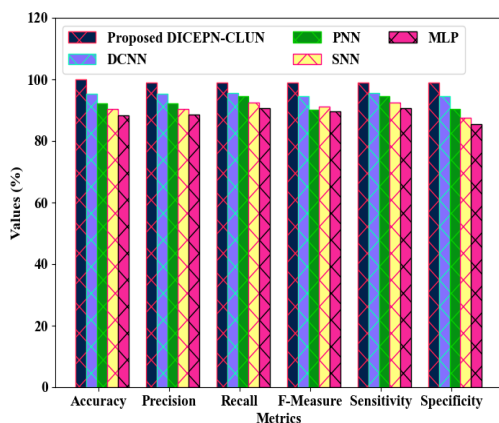


Fig.4. Performance validation of the proposed DICEPN-CLUN

The performance of the proposed FRQWIS and the conventional algorithms like FIS, sigmoid-fuzzy, trapezoidal-fuzzy, and triangular-fuzzy is validated in Fig.3. For fuzzification, defuzzification, and rule generation, the proposed FRQWIS took 463ms, 465ms, and 680ms, while the existing algorithms took 954ms, 956ms, and 1093ms, respectively. Thus, owing to the presence of RQWM, the proposed method had low time complexity.

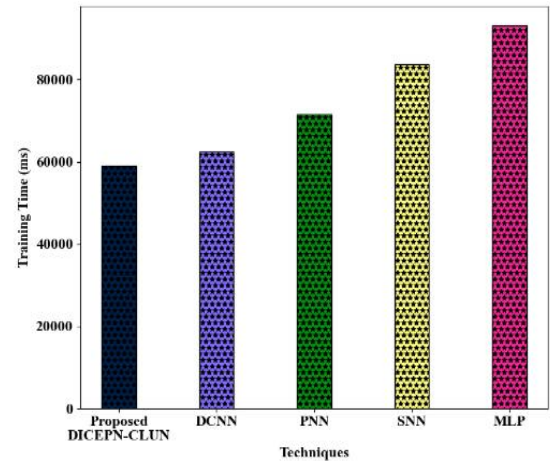


Fig.5. Training time analysis

The performance analysis for SC classification is presented in Fig.4 and Fig.5. The proposed DICEPN-CLUN's performance is weighed against the prevailing algorithms like DCNN, Probabilistic Neural Network (PNN), Spiking Neural Network (SNN), along with Multi-Layer Perceptron (MLP). For accuracy, precision, recall, f-measure, sensitivity, specificity, and training time, the proposed DICEPN-CLUN achieved 99.9046%, 98.9873%, 98.9873%, 98.9773%, 98.9873%, 98.9222%, and 58974ms, respectively. Nevertheless, the existing algorithms attained lower accuracy, precision, recall, f-measure, sensitivity, and specificity and higher training time than the proposed classifier. Therefore, owing to the presence of CosLU, the proposed method had higher supremacy.

Table.2. Cohen's kappa

Algorithm	Cohen's Kappa
Proposed DICEPN-CLUN	0.9963
DCNN	0.9217
PNN	0.8456
SNN	0.7937
MLP	0.7139

In Table 2, Cohen's kappa of the proposed DICEPN-CLUN is analyzed. For Cohen's kappa, the proposed DICEPN-CLUN attained 0.9963, whereas the existing MLP achieved 0.7139. Here, the proposed work had better efficacy.

In Fig.6, the proposed ERHF-UNet's performance is compared with prevailing UNet, Active Contour (AC), Region-Convolutional Neural Network (R-CNN), along with Faster R-CNN. The proposed ERHF-UNet achieved a dice score of 0.9824, silhouette score of 0.98239, Mean Absolute Error (MAE) of 0.0148, and Root Mean Squared Error (RMSE) of 0.258.

Moreover, the traditional UNet obtained a dice score, silhouette score, MAE, and RMSE of 0.7333, 0.92278, 0.0851, and 0.483, respectively. Therefore, the proposed work had fewer errors.

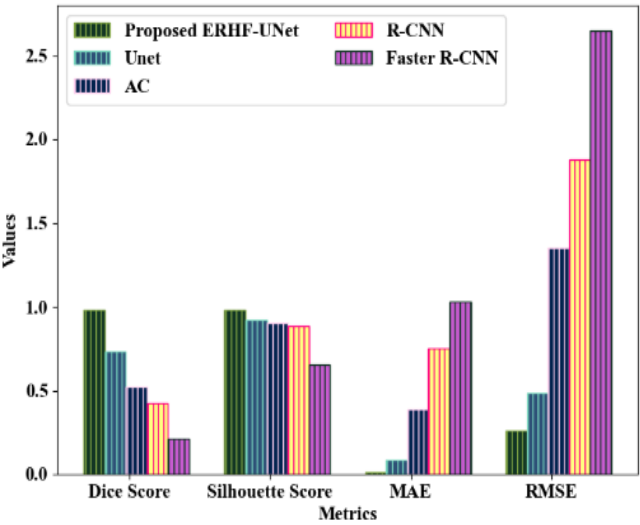


Fig.6. Performance validation for lesion segmentation

Table.3. Dataset validation

Dataset/ Metrics		DICEPN -CLUN	DCNN	PNN	SNN	MLP
ISIC- 2019	Accuracy (%)	99.9	95.3	92.2	90.4	88.3
	Precision (%)	98.99	95.3	92.3	90.4	88.6
HAM10 000	Accuracy (%)	99.87	95.2	92.1	90.1	88.1
	Precision (%)	98.78	95.1	91.9	89.9	88.3
PH ²	Accuracy (%)	99.67	94.9	91.6	89.7	87.9
	Precision (%)	98.54	94.8	91.4	89.4	88

The validation of datasets like ISIC-2019, HAM10000, and PH² for SC detection is given in Table 3. While using the ISIC-2019 dataset, the proposed DICEPN-CLUN and the existing DCNN, PNN, SNN, and MLP detected the SC with accuracy and precision values of 99.9%, 95.3%, 92.2%, 90.4%, and 88.3% and 98.99%, 95.3%, 92.3%, 90.4%, and 88.6%, respectively. Likewise, while using the HAM10000 dataset, the proposed DICEPN-CLUN and the existing DCNN, PNN, SNN, and MLP detected the SC with accuracy and precision values of 99.87%, 95.2%, 92.1%, 90.1%, and 88.1% and 98.78%, 95.1%, 91.9%, 89.9%, and 88.3%, correspondingly. Also, during the usage of the PH² dataset, the proposed method achieved an accuracy of 99.67% and a precision of 98.54%, whereas the existing techniques attained lower accuracy and precision values. Thus, regarding the datasets, such as ISIC-2019, HAM10000, and PH², the proposed model attained better performance in SC detection by comparing the proposed classifier with the existing models.

4.3 COMPARATIVE EVALUATION

Here, the comparative assessment of the proposed work (DICEPN-CLUN) is done by comparing it with existing techniques like Federated Learning-based CNN [20], CNN [21], hyper parameter-optimized full resolution convolutional network [22], deep neural network with modified EfficientNet [23], DCNN [24], and hybrid DL [25]. The proposed DICEPN-CLUN obtained an accuracy of 99.9046%, precision of 98.9873%, and sensitivity of 98.9873%. However, the prevailing [20] attained an accuracy, precision, and recall of 96.6%, 96.7%, and 92.6%, respectively. Also, the existing [25] had accuracy, precision, and sensitivity of 96.10%, 88.69%, and 88.90%, respectively. Therefore, the proposed model had effective performance in SC classification.

4.4 K-FOLD VALIDATION

In this phase, the K-Fold cross-validation is used to assess the generalizability of the dataset used in this work. This validation helps to reduce the overfitting issue and improves the performance of the model for unseen data.

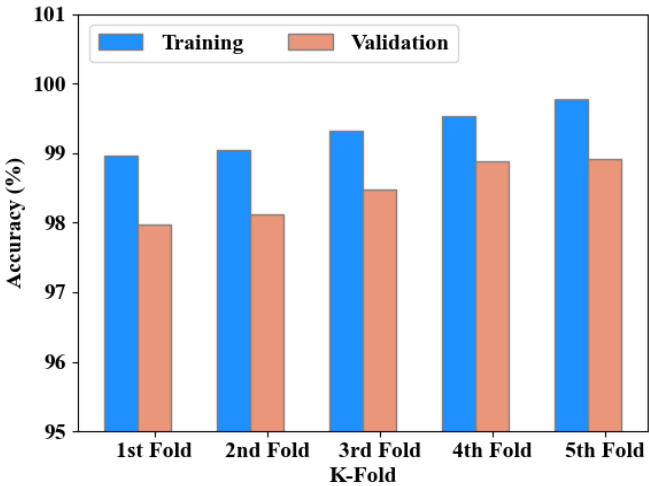


Fig.7. K-Fold Cross Validation Analysis

As depicted in Fig.7, the K-Fold cross-validation, such as 1st, 2nd, 3rd, 4th, and 5th Fold for the ISIC-2019 dataset attained training accuracies of 98.96%, 99.04%, 99.32%, 99.53%, and 99.78% and validation accuracies of 97.97%, 98.12%, 98.48%, 98.89%, and 98.91%, respectively. Hence, the proposed DICEPN-CLUN classifier performed better across different K-Folds, thus showing more stable and realistic estimates regarding SC classification.

4.5 STATISTICAL ANALYSIS

The validation of the proposed work regarding the statistical analysis is illustrated in Fig.8.

The p-value of 0.0210 with a threshold of 0.0461 indicated that the proposed system’s observed results were unlikely due to the random variations. This p-value also proved that the proposed work showed statistical improvements. Hence, the efficacy of the proposed approach validated the robustness of the model.

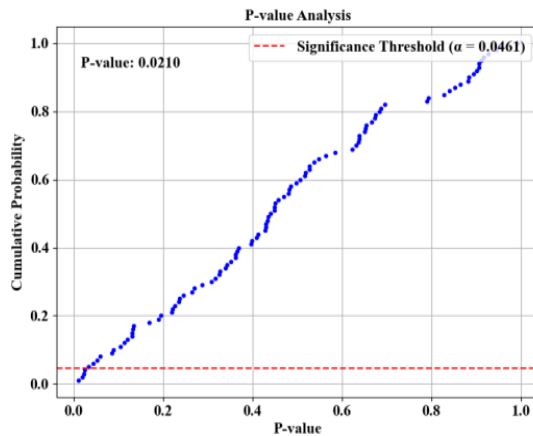


Fig.8. Statistical Performance Analysis

5. CONCLUSION

In this paper, a robust DICEPN-CLUN-based pitting/crusting ratio estimation and multiclass SC classification using dermoscopy images was proposed. The pitting/crusting ratio was efficiently estimated in the proposed work. Furthermore, the eight categories of SC were classified by the proposed DICEPN-CLUN. As per the evaluation outcomes, the proposed work obtained accuracy and MAE of 99.9046% and 0.0148, respectively. Overall, in SC classification, the proposed work had promising findings.

5.1 FUTURE SCOPE

Multimodalities will include Reflectance Confocal Microscopy (RCM) and histopathological images in the future to classify the SC.

REFERENCES

- [1] S. Nazari and R. Garcia, "Automatic Skin Cancer Detection using Clinical Images: A Comprehensive Review", *Life*, Vol. 13, No. 11, pp. 1-7, 2023.
- [2] R. Kaur, H. GholamHosseini, R. Sinha and M. Linden, "Automatic Lesion Segmentation using Atrous Convolutional Deep Neural Networks in Dermoscopic Skin Cancer Images", *BMC Medical Imaging*, Vol. 22, No. 1, pp. 1-13, 2022.
- [3] S.K. Singh, V. Abolghasemi and M.H. Anisi, "Fuzzy Logic with Deep Learning for Detection of Skin Cancer", *Applied Sciences*, Vol. 13, pp. 1-20, 2023.
- [4] K. Shehzad, Z. Tan, S. Shifa, A. Saeed, I. Ahmad, S.S. Bhatti and A.C. Samia, "A Deep-Ensemble-Learning-based Approach for Skin Cancer Diagnosis", *Electronics*, Vol. 12, No. 6, pp. 1-6, 2023.
- [5] A. Naeem, T. Anees, M. Khalil, K. Zahra, R.A. Naqvi and S.W. Lee, "SNC_NET: Skin Cancer Detection by Integrating Handcrafted and Deep Learning-based Features using Dermoscopy Images", *Mathematics*, Vol. 12, No. 7, pp. 1-35, 2024.
- [6] F. Grignaffini, F. Barbuto, L. Piazza, M. Troiano and F. Mangini, "Machine Learning Approaches for Skin Cancer Classification from Dermoscopic Images: A Systematic Review", *Algorithms*, Vol. 15, No. 11, pp. 1-30, 2022.
- [7] S.M. Jaisakthi, P. Mirunalini, C. Aravindan and R. Appavu, "Classification of Skin Cancer from Dermoscopic Images using Deep Neural Network Architectures", *Multimedia Tools and Applications*, Vol. 82, pp. 15763-15778, 2023.
- [8] R.O. Ogundokun, A. Li, R.B. Seyi, O.S. Peter, A.A. Tosho and A.N. Babatunde, "Enhancing Skin Cancer Detection and Classification in Dermoscopic Images through Concatenated MobileNetV2 and Xception Models", *Bioengineering*, Vol. 10, No. 8, pp. 1-13, 2023.
- [9] Z. Lan, S. Cai, X. He and X. Wen, "FixCaps: An Improved Capsules Network for Diagnosis of Skin Cancer", *IEEE Access*, Vol. 10, pp. 76261-76267, 2022.
- [10] W. Gouda, N.U. Sama, G. Al-Waakid, M. Humayun and N.Z. Jhanjhi, "Detection of Skin Cancer based on Skin Lesion Images using Deep Learning", *Healthcare*, Vol. 10, No. 7, pp. 1-8, 2022.
- [11] R. Kaur, H. GholamHosseini, R. Sinha and M. Lindén, "Melanoma Classification using a Novel Deep Convolutional Neural Network with Dermoscopic Images", *Sensors*, Vol. 22, No. 3, pp. 1-11, 2022.
- [12] D. Keerthana, V. Venugopal, M.K. Nath and M. Mishra, "Hybrid Convolutional Neural Networks with SVM Classifier for Classification of Skin Cancer", *Biomedical Engineering Advances*, Vol. 5, pp. 1-8, 2023.
- [13] S. Bakheet, S. Alsubai, A. El-Nagar and A. Alqahtani, "A Multi-Feature Fusion Framework for Automatic Skin Cancer Diagnostics", *Diagnostics*, Vol. 13, No. 8, pp.1-16, 2023.
- [14] M. Tahir, A. Naeem, H. Malik, J. Tanveer, R.A. Naqvi and S.W. Lee, "DSCC_Net: Multi-Classification Deep Learning Models for Diagnosing of Skin Cancer using Dermoscopic Images", *Cancers*, Vol. 15, No. 7, pp. 1-28, 2025.
- [15] A. Naeem, T. Anees, M. Fiza, R.A. Naqvi and S.W. Lee, "SCDNET: A Deep Learning-based Framework for the Multiclassification of Skin Cancer using Dermoscopy Images", *Sensors*, Vol. 22, No. 15, pp. 1-18, 2022.
- [16] D.K. Saha, A.M. Joy and A. Majumder, "YoTransViT: A Transformer and CNN Method for Predicting and Classifying Skin Diseases using Segmentation Techniques", *Informatics in Medicine Unlocked*, Vol. 47, pp. 1-15, 2024.
- [17] I. Pacal, M. Alaftekin and F.D. Zengul, "Enhancing Skin Cancer Diagnosis using Swin Transformer with Hybrid Shifted Window-based Multi-Head Self-Attention and SwiGLU-based MLP", *Journal of Imaging Informatics in Medicine*, Vol. 37, pp. 3174-3192, 2024.
- [18] Z. He, X. Li, Y. Chen, N. Lv and Y. Cai, "Attention-based Dual-Path Feature Fusion Network for Automatic Skin Lesion Segmentation", *BioData Mining*, Vol. 16, No. 1, pp. 1-22, 2023.
- [19] M. Bencevic, M. Habijan, I. Galic, D. Babin and A. Pizurica, "Understanding Skin Color Bias in Deep Learning-based Skin Lesion Segmentation", *Computer Methods and Programs in Biomedicine*, Vol. 245, pp. 1-10, 2024.
- [20] M.M. Yaqoob, M. Alsulami, M.A. Khan, D. Alsadie, A.K.J. Saudagar and M. AlKhathami, "Federated Machine Learning for Skin Lesion Diagnosis: An Asynchronous and Weighted Approach", *Diagnostics*, Vol. 13, No. 11, pp. 1-15, 2023.

- [21] .M. Rahman, M.K. Nasir, M. Nur-A-Alam and M.S.I. Khan, "Proposing a Hybrid Technique of Feature Fusion and Convolutional Neural Network for Melanoma Skin Cancer Detection", *Journal of Pathology Informatics*, Vol. 14, pp. 1-9, 2023.
- [22] D. Adla, G.V.R. Reddy, P. Nayak and G. Karuna, "A Full-Resolution Convolutional Network with a Dynamic Graph Cut Algorithm for Skin Cancer Classification and Detection", *Healthcare Analytics*, Vol. 3, pp. 1-16, 2023.
- [23] V. Venugopal, N.I. Raj, M.K. Nath and N. Stephen, "A Deep Neural Network using Modified EfficientNet for Skin Cancer Detection in Dermoscopic Images", *Decision Analytics Journal*, Vol. 8, pp. 1-11, 2023.
- [24] E.H. Houssein, D.A. Abdelkareem, G. Hu, M.A. Hameed, I.A. Ibrahim and M. Younan, "An Effective Multiclass Skin Cancer Classification Approach based on Deep Convolutional Neural Network", *Cluster Computing*, Vol. 27, pp. 12799-12819, 2024.
- [25] F. Olayah, E.M. Senan, I.A. Ahmed and B. Awaji, "AI Techniques of Dermoscopy Image Analysis for the Early Detection of Skin Lesions based on Combined CNN Features", *Diagnostics*, Vol. 13, No. 7, pp. 1-29, 2023.
- [26] Dataset, "Skin Lesion Images for Melanoma Classification", Available at <https://www.kaggle.com/datasets/andrewmvd/isic-2019>, Accessed in 2019.